11-15-1995

# A ROSAT HRI Observation of the Supernova Remnant G109.1 – 1.0

Alan P. Hurford
*Dartmouth College*

Robert A. Fesen
*Dartmouth College*

Mon. Not. R. Astron. Soc. **277**, 549–552 (1995)

# A *ROSAT* HRI observation of the supernova remnant G109.1 − 1.0

Alan P. Hurford★ and Robert A. Fesen†

*6127 Wilder Laboratory, Department of Physics and Astronomy, Dartmouth College, Hanover NH 03755, USA*

Accepted 1995 June 8. Received 1995 April 25

**ABSTRACT**

We present results of a search using *ROSAT* HRI data for X-ray spatial substructures in the galactic supernova remnant G109.1 − 1.0 which might indicate a connection between the remnant's bright X-ray blob and its X-ray pulsar, 1E2259 + 586. A 0.1–2.4 keV HRI image, created by combining separate 28- and 22-ks pointings, reveals the presence of a few small-scale X-ray features, including a NE–SW emission ridge in the remnant's X-ray blob. Two diffuse knots in the X-ray blob, previously suggested as being aligned with the X-ray pulsar, appear to be statistical fluctuations in the *Einstein* HRI data. We find no morphological evidence in the X-ray spatial substructures of G109.1 − 1.0 to support a pulsar jet origin for the X-ray blob as proposed by Gregory & Fahlman.

**Key words:** pulsars: individual: 1E2259 + 586 – ISM: individual: G109.1 − 1.0 – supernova remnants – X-rays: ISM.

## 1 INTRODUCTION

The galactic supernova remnant (SNR) G109.1 − 1.0 was discovered independently by Gregory & Fahlman (1980) using the *Einstein* Imaging Proportional Counter (IPC) X-ray detector and by Hughes, Harten & van den Bergh (1981) during a radio survey of the galactic plane. G109.1 − 1.0 exhibits several distinctive properties, including (i) a semi-circular radio and X-ray shell [radius ≃ 18 arcmin or ≃ 21 ($D$/4 kpc)], incomplete on the western side (Hughes et al. 1984; Seward 1990); (ii) a 6.98-s X-ray pulsar, 1E2259 + 586, with no radio or optical counterpart (Fahlman & Gregory 1983; Hughes et al. 1984; Coe & Jones 1992); (iii) a bright blob of X-ray emission located mid-way between the remnant's limb-brightened shell and the X-ray pulsar, which is not detected in the radio but may be partially seen in the IR (Hughes et al. 1984; Coe et al. 1989; Seward 1990); and (iv) faint optical filaments largely restricted to the north-east and south rims near regions of strong radio emission (Hughes et al. 1981; Fesen & Hurford 1995).

The unusual semicircular appearance of G109.1 − 1.0 has been attributed to the interaction of the SNR with a large molecular cloud complex situated to the west. This interpretation is supported by CO emission maps and *IRAS* scan data of the remnant and cloud complex (Tatematsu et al. 1987, 1990; Coe et al. 1989), and by numerical hydrodynamical simulations of a supernova (SN) event near the edge of a large molecular cloud (Tenorio-Tagle, Bodenheimer & Yorke 1985; Yorke et al. 1989; Wang et al. 1992). A molecular ridge (CO arm) extending eastward from the cloud complex may absorb some of the remnant's north-central X-ray emission, but without significantly altering the overall X-ray appearance of the SNR (Tatematsu et al. 1990).

To explain the X-ray and radio morphology of G109.1 − 1.0, Gregory & Fahlman (1983) proposed that the X-ray pulsar ejects two oppositely directed, precessing jets. They interpreted the radio structure of the remnant as comprising two intersecting arcs representing the trace of the interactions of the jets with the SNR shell. Radio peaks on the north-east and south rims of the remnant were suggested as indicating where the jets currently interact with the cavity wall. The bright X-ray blob, which lies along the proposed precession axis, was interpreted as either jet-excited material inside the remnant or emission from one of the jets itself.

Coe & Jones (1992), in a re-analysis of an *Einstein* High Resolution Imager (HRI) image of 1E2259 + 586, found two diffuse knots in the X-ray blob aligned with the pulsar, indicating the possible presence of a pulsar jet. However, recent analysis of *ROSAT* PSPC spectral data shows only thermal emission from the X-ray blob with no evidence of synchrotron radiation (Rho & Petre 1993), greatly reducing the likelihood of a jet. The thermal spectrum of the X-ray blob instead supports suggestions that the blob is either a shocked cloud at the outskirts of the CO arm (Tatematsu et al. 1990) or hot, shocked molecular cloud gas streaming away from the SN explosion site (Tenorio-Tagle et al. 1985).

This paper presents the results of our search for X-ray spatial substructures in G109.1 − 1.0 that might indicate a

★ E-mail: hurford@nebula.dartmouth.edu
†E-mail: fesen@oak.dartmouth.edu

connection between the bright X-ray blob and the X-ray pulsar. We also discuss the significance of the diffuse knots seen in the earlier *Einstein* HRI image in view of the more recent *ROSAT* HRI and Position Sensitive Proportional Counter (PSPC) observations.

## 2 OBSERVATIONS

A 28-ks *ROSAT* HRI observation of G109.1 − 1.0, pointed at the bright X-ray blob of the remnant was obtained in 1992 June 25–27. This pointing enabled us to resolve as well as possible any internal blob structure, while the large field-of-view of the HRI ($36 \times 36$ arcmin$^2$) also yielded good imaging of most other regions of the SNR. The HRI has a spatial resolution (telescope plus detector) ranging from $\simeq 5$ arcsec on-axis to $\simeq 30$ arcsec at 15 arcmin off-axis, and a 0.1–2.4 keV bandpass with peak sensitivity at 1.1 keV. Detailed descriptions of the *ROSAT* X-ray mirror assembly and *ROSAT* HRI detector are given by Aschenbach (1988) and Zombeck et al. (1990).

In addition, we extracted 22-ks *ROSAT* HRI and 34-ks *ROSAT* PSPC observations of G109.1 − 1.0 from the data archive. The archival HRI data, centred on the X-ray pulsar, 1E2259 + 586, $\simeq 8$ arcmin west of the X-ray blob, offers $\simeq 3$ times higher spatial resolution of the faint western boundary of the remnant and provides a confirmation for small-scale structures present in our 28-ks observation. The *ROSAT* PSPC, with $\simeq 30$ arcsec resolution over the entire SNR, a 0.1–2.4 keV bandpass with peak sensitivities at 0.3 keV and 1.1 keV, and a count rate $\simeq 3$ times the *ROSAT* HRI (David et al. 1993), serves as an independent check on the gross X-ray features seen by the HRI. Further information on the *ROSAT* PSPC can be found in Pfeffermann et al. (1986).

To utilize the highest resolution portions of both HRI images, we used IRAF/PROS software to create a mosaic of G109.1 − 1.0. For each data set, the X-ray photons were binned into 5 arcsec pixels (no significant smaller-scale spatial structures were observed) to improve the signal-to-noise ratio, and the resulting images were background-subtracted and vignetting-corrected (at 1.1 keV). After scaling the 22-ks exposure time of the archival data to match our own 28-ks observation, the two images were mosaiced along a north–south line $\simeq 1.5$ arcmin east of the X-ray pulsar, and the resulting mosaic smoothed using a 2D Gaussian fit with FWHM = 15 arcsec. For the PSPC data set, the X-ray photons were also binned into 5 arcsec pixels, and the resulting image background-subtracted, vignetting-corrected (at 1.1 keV), and smoothed using a 2D Gaussian fit with FWHM = 30 arcsec.

Finally, to enable a direct comparison with the more recent *ROSAT* HRI and PSPC data, we obtained the archival 21-ks *Einstein* HRI observation. This image, centred $\simeq 3.5$ arcmin south-west of the X-ray pulsar, includes all but the north-east portion of the bright X-ray blob (as a result of the smaller $25 \times 25$ arcmin$^2$ field-of-view). Although the *Einstein* HRI had a resolution of 5–6 arcsec at the 10–13 arcmin off-axis angle of the X-ray blob, the associated 10–20 arcsec half-power radius caused substantial scattering of X-ray photons, resulting in a poor detection of this feature. In addition, the lower quantum efficiency of the *Einstein* HRI microchannel plates leads to a count rate in the 0.15–4.0 keV bandpass typically $\simeq 1/3$ that of the *ROSAT* HRI (David et al. 1993). A detailed description of the *Einstein* HRI is given by Giacconi et al. (1979). Following Coe & Jones (1992), the X-ray photons for the four data sets were binned into 2 arcsec pixels and the resulting images smoothed using a 2D Gaussian fit with FWHM = 30 arcsec.

## 3 RESULTS AND DISCUSSION

### 3.1 X-ray spatial features

The composite *ROSAT* HRI image of G109.1 − 1.0 is presented in Fig. 1 (opposite p. 550). This represents the highest resolution X-ray image of the remnant presented to date, offering two (on-axis) to five (off-axis) times greater resolution over the *Einstein* IPC data (3600-s exposure, FWHM $\simeq 1.25$ arcmin, bandpass 0.3–4.5 keV; Seward 1990), and about twice that of the *ROSAT* PSPC. The brightest features in G109.1 − 1.0 are the X-ray pulsar, 1E2259 + 586, followed by the triangular-shaped X-ray blob or 'X-ray jet' (Gregory & Fahlman 1983) located $\simeq 8$ arcmin east of the pulsar, and the regions of enhanced X-ray emission along the north-east and south-east rims. Also evident are the well-defined eastern shell emission and the faint western boundary. Diffuse X-ray emission permeates the interior of the remnant. These gross HRI features are similar to those seen in both the IPC image (Seward 1990) and the archival PSPC data (Fig. 2, opposite p. 550). Three point sources present in Fig. 1, two inside and one outside of the SNR, do not appear to be associated with G109.1 − 1.0, and so are not discussed further.

The composite HRI image also shows numerous small-scale emission clumps, most of which are confined to the north-east and south-east limb-brightened shell and the bright X-ray blob. Generally, these features are associated with larger-scale bright emission patches seen in the PSPC data. Poor spatial correspondence exists between clumps seen in the individual 28- and 22-ks HRI data sets, however, indicating that many are not real but simply statistical fluctuations in the bright PSPC regions. Five of the brightest clumps appear to form a well-aligned, regularly spaced chain (separation $\simeq 1$ arcmin, PA $\simeq 35°$; see Fig. 1) within the X-ray blob. Again, however, examination of the archival 22-ks HRI data fails to confirm the existence of this unusual feature. The more sensitive PSPC detector also failed to resolve these clumps in either soft (0.1–0.5 keV) or hard (0.5–2.4 keV) energy bands, despite their sufficient spacing.

On the other hand, the PSPC image (Fig. 2) does show a broad NE–SW emission ridge within the X-ray blob surrounding these five clumps. Also, the brighter central clumps in this chain correspond to the brightest regions of the X-ray blob as seen by the PSPC. Because the relative sensitivity of the PSPC at soft versus hard energies is greater than for the HRI, these five clumps are probably statistical fluctuations in a soft X-ray emission ridge that is relatively poorly detected by the HRI. This suggested softness for the X-ray emission ridge is consistent with the PSPC spectral analysis carried out by Rho & Petre (1993). They find the X-ray blob to be the softest feature in G109.1 − 1.0, having a spectrum best-fitted by a two-temperature thermal model with components $(0.13–0.14) \pm 0.05$ keV and $(0.29–0.31) \pm 0.05$ keV.

Opposite p. 550, MNRAS, 277

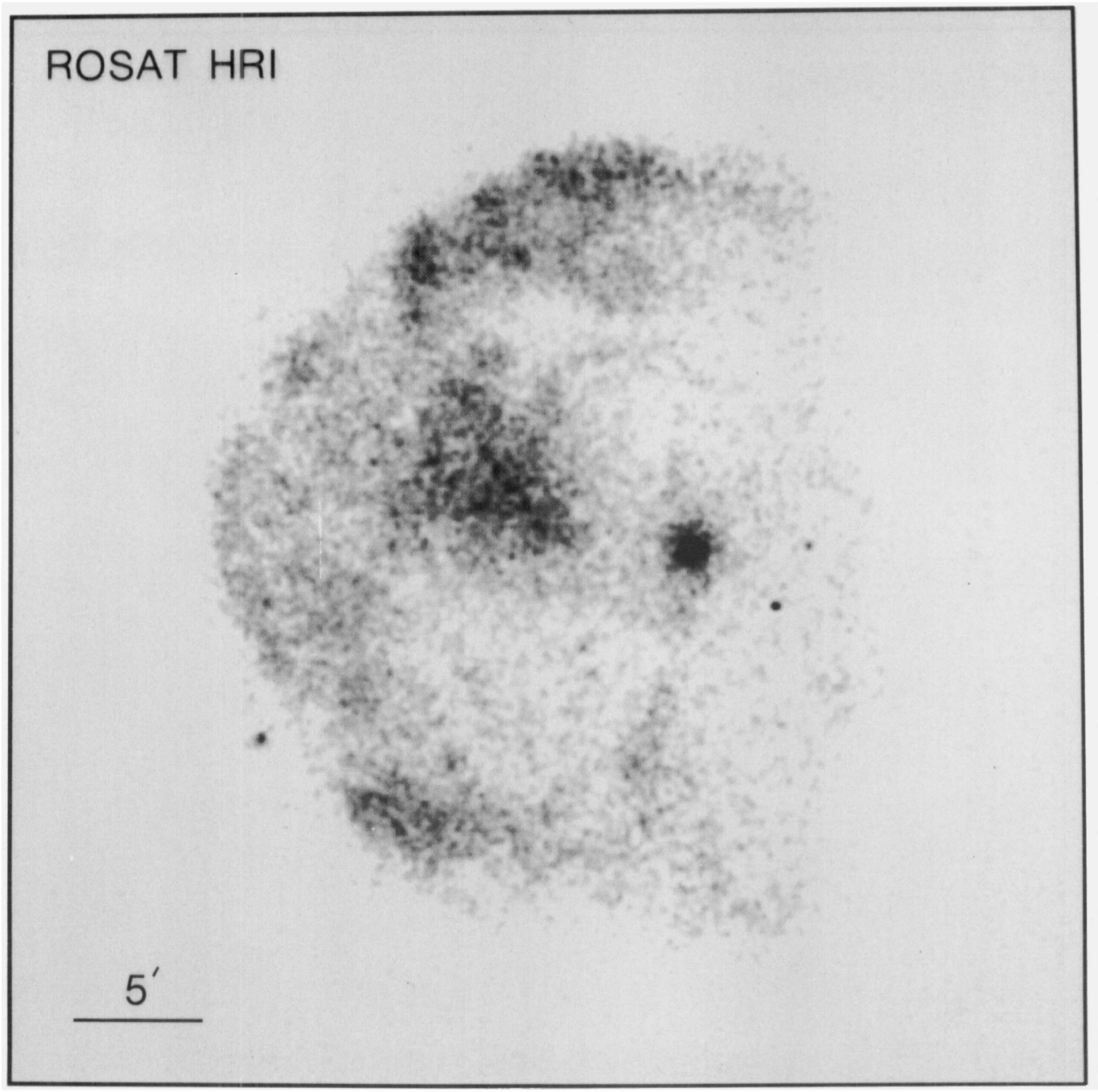


**Figure 1.** Composite *ROSAT* HRI image of G109.1 − 1.0 at a resolution (FWHM) of 15 arcsec. The bright point source west of centre is the X-ray pulsar, 1E2259 + 586. North is up, east is to the left.

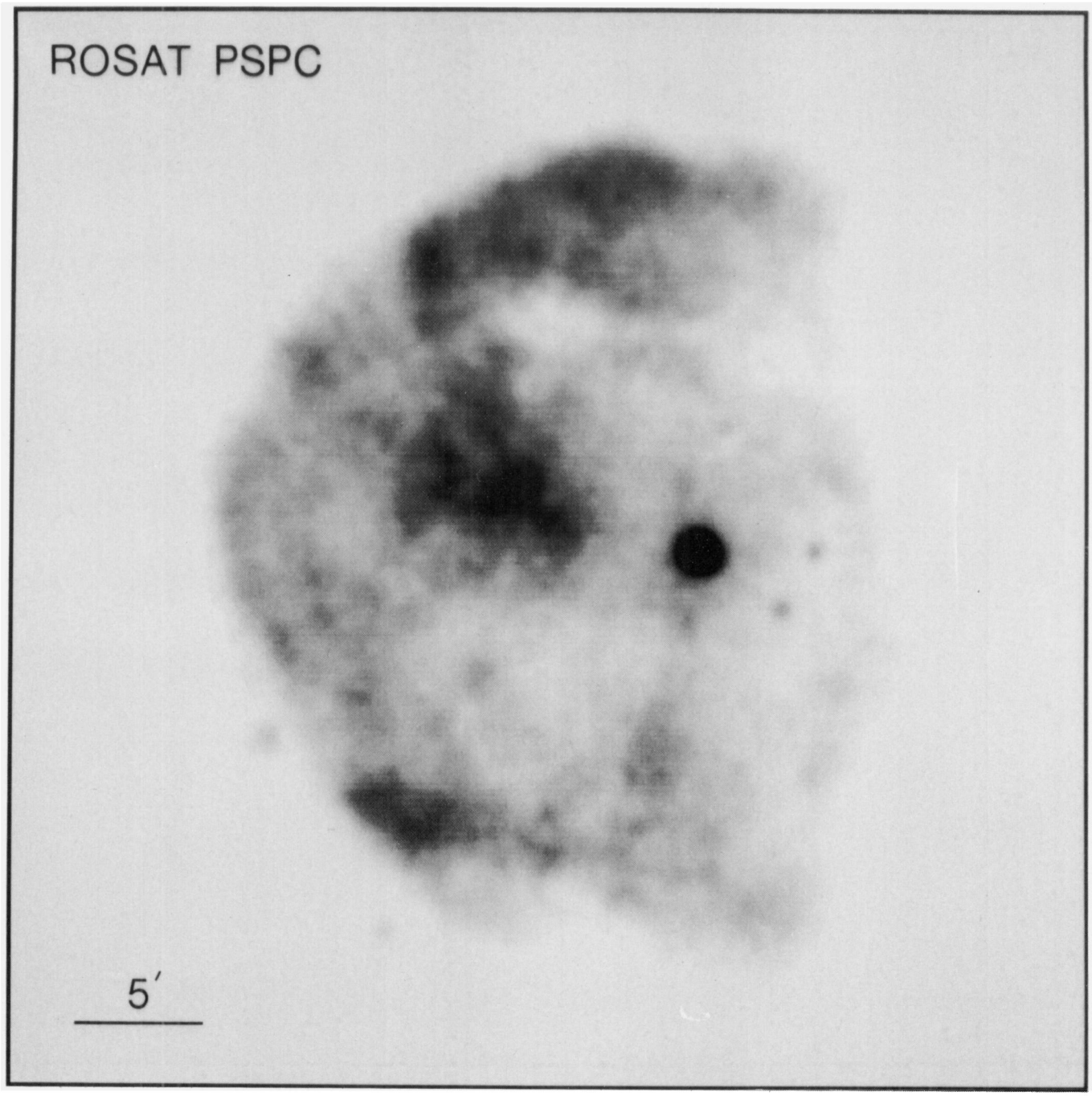


**Figure 2.** *ROSAT* PSPC image of G109.1 − 1.0 at a resolution (FWHM) of 30 arcsec.

1995MNRAS.277..549H

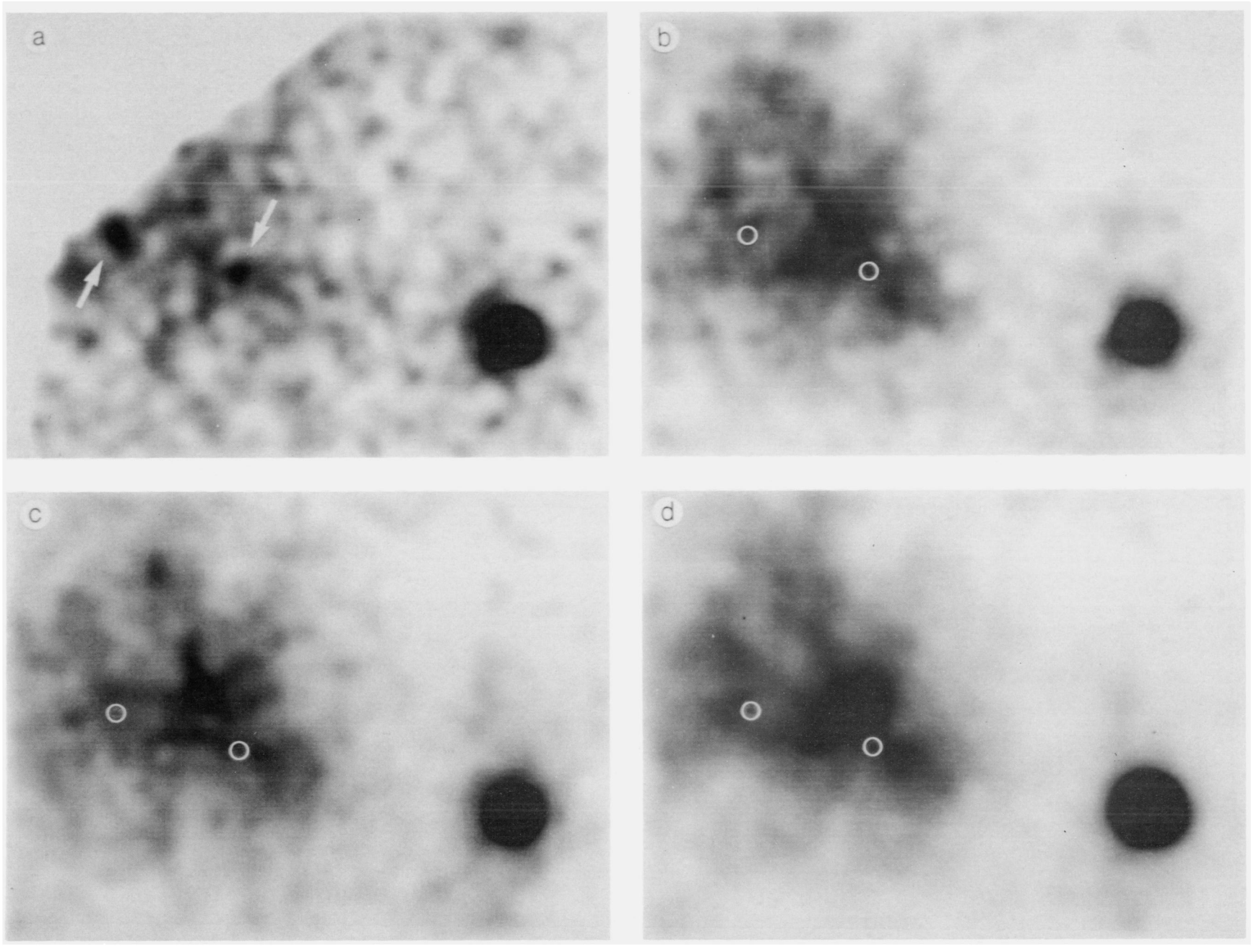


**Figure 3.** Four X-ray images of an $\simeq 14 \times 11$ arcmin$^2$ region around the pulsar and X-ray blob (FWHM = 30 arcsec). Panel (a) shows the 21-ks *Einstein* HRI image, with white arrows identifying the two diffuse knots found by Coe & Jones (1992). Panels (b) and (c) show the 28-ks and 22-ks *ROSAT* HRI images, while panel (d) shows the 34-ks *ROSAT* PSPC image. The small white circles indicate the locations of the two Coe & Jones (1992) knots in the *ROSAT* HRI and PSPC images. Note that the north-east portion of the X-ray blob in Fig. 3(a) is cut off by the smaller field of view of the *Einstein* HRI.

### 3.2 Evidence for an X-ray jet?

The bright X-ray blob in G109.1 − 1.0 has been proposed as being either emission from a jet off the X-ray pulsar, 1E2259 + 586, or jet-excited gas inside the remnant shell (Gregory & Fahlman 1983). In the PSPC image (Fig. 2), the emission ridge within the X-ray blob, while unaligned with the X-ray pulsar, does appear to curl somewhat at its southern tip towards the pulsar. This could be interpreted as indicating a physical connection between the X-ray blob and the pulsar. In addition, the alignment and proximity of the emission ridge to the eastern edge of the north-east limb-brightened shell of the remnant might also suggest an association between the X-ray blob and north-east shell emission.

There are no peculiar small-scale features in the *ROSAT* images of the X-ray blob (Fig. 3, opposite p. 550), e.g., a hot-spot or a bow-shock structure close to the pulsar, however, that would suggest that the X-ray flux of the blob is excited by a pulsar jet. Also, we see no small-scale structures in the immediate vicinity of the X-ray blob or pulsar that would indicate collimated emission from 1E2259 + 586. The strongest evidence against the pulsar jet model of Gregory & Fahlman (1983) comes from the PSPC spectral data. Rho & Petre (1993) find that the X-ray blob and north-east shell possess thermal spectra, with no evidence for synchrotron emission, implying minimal influence of the pulsar on the X-ray appearance of the SNR.

Possible circumstantial evidence for a pulsar jet was reported by Coe & Jones (1992). In a re-analysis of the *Einstein* HRI data, they reported finding two diffuse X-ray knots aligned with the pulsar. In Fig. 3 we show four X-ray images of the region around the pulsar and X-ray blob: (a) the 21-ks *Einstein* HRI image; (b) our 28-ks *ROSAT* HRI image; (c) the archival 22-ks *ROSAT* HRI image; and (d) the 34-ks *ROSAT* PSPC image. Note that the north-east portion of the X-ray blob in Fig. 3(a) is cut off by the smaller field of view of the *Einstein* HRI. Although two emission clumps in the 28-ks *ROSAT* HRI image approximately coincide with these two diffuse knots, the *Einstein* HRI image (centred ≃ 3.5 arcmin south-west of the pulsar) does not show some brighter clumps that were seen in the *ROSAT* HRI image (centred on the X-ray blob). The archival *ROSAT* HRI and PSPC observations also fail to confirm the existence of these diffuse X-ray knots, further arguing against the reality of these small-scale features. Unless the diffuse knots detected by Coe & Jones possess unusually hard spectra, favouring their detection by the *Einstein* HRI (0.15–4.0 keV) over the *ROSAT* HRI (0.1–2.4 keV), it is likely these two features are only statistical fluctuations in the bright X-ray blob emission.

Thus, while we are unable to completely rule out the existence of these two diffuse knots, the weight of the new *ROSAT* HRI and PSPC data indicates they are not real features. The pulsar jet model proposed by Gregory & Fahlman (1983) to explain the major radio and X-ray morphological features of G109.1 − 1.0 is also not supported by either high-resolution X-ray imaging or X-ray spectral data.

### 3.3 Alternative explanations for the X-ray emission structure

An alternative explanation for the unusual X-ray morphology of G109.1 − 1.0 has been proposed by Tenorio-Tagle et al. (1985). From numerical hydrodynamical models of a SN located just inside a large molecular cloud, they found that a SNR breaking out of the cloud during its adiabatic phase can produce a mushroom-like X-ray morphology when viewed edge-on. In their models, the top of this X-ray mushroom feature results from matter recently encountered by the expanding shock, while the stem comprises hot shocked molecular cloud material swept up early in the SNR's evolution. Tenorio-Tagle et al. identified the X-ray blob and X-ray shell in G109.1 − 1.0 with the stem and the top of this mushroom-like structure, respectively.

Support for this picture may come from the radio morphology of the remnant. The 21- and 49-cm radio maps of Hughes et al. (1984) show that the radio structure of G109.1 − 1.0 exhibits a similar mushroom-like shape. While the radio shell emission is likely to be a result of synchrotron emission from relativistic particles in the swept-up interstellar magnetic field, a radio emission 'stem', which runs eastward from the molecular cloud to the western edge of the X-ray blob, could be cooler, shocked gas streaming away from the supernova site. The weak radio emission observed near the X-ray blob may reflect a less compressed magnetic field in this region.

This cloud break-out model, while possibly explaining the gross X-ray structure of the remnant, does not explicitly account for the bright radio lobes seen along the north-east and south rims. These features may mark the interaction of the SN blast wave with H II regions in these areas. New optical imaging shows that the filaments of G109.1 − 1.0 may lie either adjacent to or embedded within the outskirts of faint H II regions (Fesen & Hurford 1995). Spectra of some of the northern and southern filaments of the SNR show relatively high electron densities, $n_e = 400$–$800$ cm$^{-3}$, implying fairly high pre-shock cloud densities, $n_c = 10$–$20$ cm$^{-3}$ (Blair & Kirshner 1981; Fesen & Hurford 1995). These relatively high pre-shock densities, together with similar filament and H II region extinction values and the locations of the filaments of the remnant near the H II region boundaries, point to possible interactions of the SNR shock with these H II regions. Such interactions could lead to the radio peaks observed in these regions.

If this shock interaction picture is correct, then the enhanced X-ray emission seen along the north-east and south-east rims of G109.1 − 1.0 (Figs 1 and 2) may likewise be a result of SNR–H II region interactions in these areas. The X-ray blob might also represent a shock interaction with a southward extension of the northern H II region. Newly discovered optical filaments located near the X-ray blob may be regions of more dense, shocked gas associated with this bright X-ray feature. Evidence supporting a shocked cloud origin for the X-ray blob is strong *IRAS* 60-μm emission located between the X-ray blob and north-east shell emission (Coe et al. 1989). In the SNR IC 443, Burton et al. (1990) found that [O I] 63-μm emission from dense shocked clouds can contribute up to 75 per cent of the total *IRAS* 60-μm band flux. The location of this 60-μm feature at the eastern edge of a CO arm extending from the western molecular cloud complex (Tatematsu et al. 1990) is consistent with a shocked cloud origin for this emission.

In summary, we find no morphological evidence in the *ROSAT* data to support the suggestion that directed pulsar emission is responsible for the major X-ray and radio

emission features in G109.1 − 1.0 (Gregory & Fahlman 1983). We are also unable to confirm the existence of two diffuse knots in the X-ray blob aligned with the pulsar (Coe & Jones 1992). Alternative explanations for the unusual X-ray emission structure of G109.1 − 1.0 include SNR breakout at the edge of a large molecular cloud and shock interaction with neighbouring H II regions.

## ACKNOWLEDGMENTS

We thank J.-H. Rho and R. Petre for generously sharing their *ROSAT* PSPC results on G109.1 − 1.0 prior to publication, and A. J. S. Hamilton for valuable comments on an earlier version of this paper. This work was sponsored in part by NASA Grant 5-2138.

## REFERENCES

Aschenbach B., 1988, Appl. Opt., 17, 1404
Blair W. P., Kirshner R. P., 1981, Nat, 291, 132
Burton M. G., Hollenbach D. J., Haas M. R., Erickson E. F., 1990, ApJ, 355, 197
Coe M. J., Jones L. R., 1992, MNRAS, 259, 191
Coe M. J., Davies S. R., Fahlman G. G., Gregory P. C., 1989, MNRAS, 238, 649
David L. P., Harnden F. R., Jr, Kearns K. E., Zombeck M. V., 1993, Addendum to Appendix F: ROSAT Mission Description. US *ROSAT* Science Data Centre/SAO, 23
Fahlman G. G., Gregory P. C., 1983, in Danziger J., Gorenstein P., eds, IAU Symp. 101, Supernova Remnants and their X-Ray Emission. Reidel, Dordrecht, p. 445
Fesen R. A., Hurford A. P., 1995, AJ, 110, 747
Giacconi R. et al., 1979, ApJ, 230, 540
Gregory P. C., Fahlman G. G., 1980, Nat, 287, 805
Gregory P. C., Fahlman G. G., 1983, in Danziger J., Gorenstein P., eds, IAU Symp. 101, Supernova Remnants and their X-Ray Emission. Reidel, Dordrecht, p. 429
Hughes V. A., Harten R. H., Costain C. H., Nelson L. A., Viner M. R., 1984, ApJ, 283, 147
Hughes V. A., Harten R. H., van den Bergh S., 1981, ApJ, 246, L127
Pfeffermann E. et al., 1986, Proc. SPIE, 733, 519
Rho J.-H., Petre R., 1993, in Contributions to the ROSAT Science Symposium and Data Analysis Workshop. University of Maryland, p. 41
Seward F. D., 1990, ApJS, 73, 781
Tatematsu K., Fukui Y., Nakano M., Kogure T., Ogawa H., Kawabata K., 1987, A&A, 184, 279
Tatematsu K., Fukui Y., Iwata T., Seward F. D., Nakano M., 1990, ApJ, 351, 157
Tenorio-Tagle G., Bodenheimer P., Yorke H. W., 1985, A&A, 145, 70
Wang Z., Qu Q., Luo D., McCray R., MacLow M.-M., 1992, ApJ, 388, 127
Yorke H. W., Tenorio-Tagle G., Bodenheimer P., Rozyczka M., 1989, A&A, 216, 207
Zombeck M. V. et al., 1990, Proc. SPIE, 1344, 267